Unresolved recombination intermediates lead to ultra-fine anaphase bridges, chromosome breaks and aberrations

Ying Wai Chan, **Kasper Fugger**, and **Stephen C. West**[1]
The Francis Crick Institute, 1 Midland Road, London NW1 1AT, UK

Abstract

The resolution of joint molecules that link recombining sister chromatids is essential for chromosome segregation. Here, we determine the fate of unresolved recombination intermediates that arise in *GEN1*^{-/-} knock-out cells depleted for MUS81, the two nucleases required for resolution. We find that intermediates persist until mitosis where they form a distinct class of anaphase bridges, which we term homologous recombination ultra-fine bridges, or HR-UFBs. The HR-UFBs are distinct from replication stress-associated UFBs, that arise at common fragile sites, and from centromeric UFBs. HR-UFBs are processed by BLM helicase to generate single-stranded RPA-coated bridges that are broken at mitosis. In the next cell cycle, DNA breaks activate the DNA damage checkpoint and chromosome fusions arise by non-homologous end joining. Consequently, the cells undergo a cell cycle delay and massive cell death. These results lead us to present a model detailing how unresolved recombination intermediates can promote DNA damage and chromosomal instability.

Proper chromosome segregation depends on the removal of all physical connections between sister chromatids prior to anaphase. These connections can be proteinaceous, such as cohesin linkages1, or might be mediated through DNA bridges that are a potential source of genome instability2. Sister chromatid non-disjunction can manifest as fine DNA strands between segregating DNA masses, referred to as ultra-fine DNA bridges (UFBs) that cannot be visualized using standard DNA dyes (e.g. DAPI), but can be detected by immunofluorescence staining for proteins, such as PICH, BLM and RPA, that bind the bridge3–6. Three major types of UFB have been described7: (i) The most common originate in centromeric regions (C-UFBs), and involve double-stranded catenanes that are resolved by topoisomerase II8, 9; (ii) UFBs can arise from late replication intermediates at common fragile sites (CFSs) following replication stress (FS-UFBs), and are characterized by the presence of twin FANCD2 repair foci7, 10–13; and (iii) telomeric UFBs (T-UFBs) in which replication stalling or fusion events occur at telomeric sequences14–16.

[1]Corresponding author: tel +(44)-203-7962071, stephen.west@crick.ac.uk.

Intermediates of homologous recombination (HR), provide a covalent link between sister chromatids and cause chromosome segregation defects if not removed before anaphase[17]. In human cells, multiple mechanisms have evolved to process recombination intermediates. One involves the BTR complex (BLM-TOPOIIIα-RMI1-RMI2), which mediates the dissolution of double Holliday junctions (HJs)[18]. Persistent double HJs and other types of recombination intermediates (e.g. single HJs, D-loop structures) that are refractory to dissolution are resolved by structure-selective endonucleases (SSEs). The SSEs include MUS81-EME1[19, 20], SLX1-SLX4[21–23] and GEN1[24–26]. SLX1-SLX4 forms a complex with MUS81-EME1 and a third nuclease, XPF-ERCC1, to form the SMX tri-nuclease complex[27, 28]. The SMX complex and GEN1 cleave recombination intermediates in two genetically distinct resolution pathways[17, 28–31].

Distinct regulatory mechanisms restrain the actions of the SSEs to the later stages of the cell cycle. SMX complex formation occurs at prometaphase following CDK1/PLK1-directed phosphorylation of MUS81-EME1 and SLX4[28, 32]. SMX complex formation activates MUS81-EME1 for the cleavage of persistent recombination and replication intermediates[27]. GEN1 acts later in the cell cycle, as this primarily cytoplasmic protein gains access to the remaining DNA intermediates after breakdown of the nuclear envelope at mitotic entry[33, 34]. Cells defective for resolution exhibit chromosome segregation errors and reduced viability[17,28–31].

Here, we establish a "resolvase-deficient" model system to detail what happens when cells with unresolved recombination intermediates enter mitosis. We find that recombination intermediates give rise to UFBs that we term homologous recombination-UFBs (HR-UFBs). BLM helicase activity is required for the conversion of the recombination intermediates into RPA-coated single-stranded bridges that are broken upon cell division, leading to chromosome aberrations and activation of the DNA damage checkpoint in the next cell cycle.

Results

Resolvase-deficiency promotes cell cycle arrest and cell death

To determine the consequences of aberrant mitosis caused by unresolved recombination intermediates, we established a 'resolvase-deficient' experimental system in cultured human cells by siRNA-depleting MUS81 from a $GEN1^{-/-}$ k/o cell line generated from 293 cells using CRISPR/Cas9[34] (Fig. 1a). These resolvase-deficient cells exhibited a reduced frequency of sister chromatid exchanges (SCEs) compared with $GEN1^{-/-}$ cells, or MUS81-depleted normal cells (Supplementary Fig. 1a). These data confirm that resolvases are responsible for generating crossovers[17, 28–31].

The resolvase-deficient cells revealed a series of striking phenotypic properties. Firstly, we observed an accumulation of cells with 4N DNA content (Fig. 1b,c). To confirm G2 arrest, cells were treated with antibodies against cyclin B (a G2 marker) and histone H3 pSer10 (a mitotic marker), and analysed by FACS (Fig. 1d). A significant increase in cyclin B-positive cells, but not histone H3 pSer10-positive cells was observed. G2 arrest occurred 96 hours after MUS81 siRNA treatment of the $GEN1^{-/-}$ cells (Supplementary Fig. 1b), indicating the

accumulation of endogenous DNA damage. Furthermore, clonogenic assays showed massive synthetic lethality (<10% cell survival) (Fig. 1e). Loss of viability and G2 arrest were rescued by exogenous expression of FLAG-tagged GEN1 (Fig. 1e and Supplementary Fig. 1c,d). The resolvase-deficient cells were highly sensitive to the DNA damaging agents cisplatin and camptothecin (CPT) (Fig. 1f and Supplementary Fig. 1e), but only mildly sensitive to replication stress induced by aphidicolin (APH) (Supplementary Fig. 1f). These results are consistent with the involvement of MUS81-EME1 and GEN1 in the resolution of DNA repair intermediates.

To gain further insights into the interplay between GEN1 and components of the SMX complex (in particular MUS81-EME1 and SLX1-SLX4), *MUS81*^{-/-} and *SLX1*^{-/-} k/o cells were generated using CRISPR/Cas9 (Supplementary Fig. 1g-i). While depletion of GEN1 from *MUS81*^{-/-} cells induced massive cell death and severe G2 arrest (Supplementary Fig. 2a,b), a less significant effect was seen in GEN1 cells depleted for *SLX1*^{-/-}. This indicates that SLX1 may only be required for the resolution of a subset of repair intermediates. Consistent with this, G2 arrest and lethality was further exacerbated by depletion of SLX1 from *GEN1*^{-/-} cells co-depleted for MUS81 (Supplementary Fig. 2c,d).

The interaction of MUS81 with the SLX4 scaffold protein is known to be critical for its resolution functions[27, 30, 31, 35]. We therefore mutated the key conserved residues in SLX4 (E1577A, L1578A) equivalent to those previously identified in mouse SLX4 that abolish MUS81-SLX4 interactions[30] (Supplementary Fig. 2e), and observed that depletion of GEN1 from SLX4[E1577A L1578A] (SLX4[ELAA]) cells induced cell death and cell cycle arrest (Supplementary Fig. 2f-h). These results confirm the synthetic relationship between GEN1 and MUS81/SLX4.

Unresolved recombination intermediates form ultra-fine bridges

To investigate the consequences of mitosis with unresolved recombination intermediates, we briefly treated resolvase-deficient cells with cisplatin and prepared metaphase spreads 24h later. We observed tightly-associated sister chromatids that exhibited a segmented appearance (Fig. 1g,h). This unusual morphology was previously attributed to defects in chromosome condensation at sites of sister chromatid entanglements[17, 29, 31]. Elevated levels of chromosome segmentation were observed even in the absence of exogenous damage (Supplementary Fig. 3a). Segmentation was suppressed by expression of the bacterial resolvase RusA fused to catalytic-dead GEN1 (with E134A, E136A mutations) to ensure correct cellular regulation, but not by catalytic-dead RusA[D70N]-GEN1 (Fig. 1i, Supplementary Fig. 3b,c). Indeed, RusA[WT]-GEN1 rescued all other phenotypes associated with resolvase deficiency, namely reduced SCE formation (Supplementary Fig. 3d) and G2 arrest (Supplementary Fig. 3e). These results show that the uncondensed regions arise from unresolved intermediates that interlink sister chromatids.

Since unresolved recombination intermediates do not trigger a cell cycle checkpoint the sister-chromatid linkages persist to anaphase. Consequently, ~80% of the resolvase-deficient cells (undamaged or cisplatin-treated) displayed RPA-decorated UFBs at anaphase/telophase, compared to ~10-15% in control and single-resolvase depleted cells (Fig. 2a,b and Supplementary Fig. 3f-h). The binding of RPA indicates that the bridges contain single-

stranded DNA (ssDNA). Previously, it was shown that mild replication stress (e.g. low dose aphidicolin) leads to unresolved replication intermediates at CFSs that give rise to FS-UFBs exhibiting RPA and BLM staining, and with twin FANCD2 foci at their termini[5, 10, 11]. In contrast to FS-UFBs, we observed UFBs that were not flanked by FANCD2 (~5% of mock-depleted wild-type cells and ~70% of the resolvase-deficient cells displayed FANCD2-negative UFBs) (Fig. 2a,b and Supplementary Fig. 3f-h). The homologous recombination UFBs therefore appear to represent a distinct class of ultrafine bridge, which we term HR-UFBs.

To determine whether UFBs that arise in resolvase-deficient 293 cells are representative of those in all cell types, we depleted GEN1 and MUS81 from the non-transformed diploid cell line hTERT-RPE1. Again, we observed an increase in FANCD2-negative UFBs compared with control and single-resolvase depleted cells (Fig. 2g,h and Supplementary Fig. 3i). These HR-UFBs did not associate with centromeres, as detected by CREST staining (Supplementary Fig. 3j).

In addition to RPA, the UFBs were also decorated with BLM (Supplementary Fig. 4a,b). To confirm that the RPA/BLM-coated UFBs did not associate with FANCD2 foci or centromeres, we co-stained for RPA/BLM and either FANCD2 or CREST using U2OS cells depleted for MUS81 and GEN1 (Supplementary Fig. 4a,b). We again observed that the majority of the RPA/BLM-coated UFBs did not associate with FANCD2 (41/49 UFBs were FANCD2 negative: 20 cells counted) or centromeres (34/47 UFBs failed to show any association with CREST: 20 cells counted).

To provide further support for the distinction between HR-UFBs and FS-UFBs, we investigated whether FANCD2 twin foci and DNA synthesis (as indicated by EdU incorporation)[12, 13, 36], occur at prometaphase in the resolvase-deficient cells. As expected, control cells treated with aphidicolin exhibited an increased frequency of FANCD2 twin foci and EdU foci on their mitotic chromosomes (Fig. 2c,d and Supplementary Fig. 4c,d), whereas brief cisplatin treatment of the resolvase-deficient cells did not lead to detectable replication stress (FANCD2 and EdU staining). Moreover, DNA fibre analysis indicated that unchallenged resolvase-deficient cells did not show reduced replication progression (Fig. 2e,f), confirming that the HR-UFBs are not induced by replication stress.

To extend our analysis of HR-UFBs, we compared resolvase-deficient cells treated with aphidicolin or camptothecin, which causes replication fork collapse and DSB formation (Fig. 3a,b, and Supplementary Fig. 4e,f). APH treatment increased the number of FANCD2-positive UFBs whereas the FANCD2-negative HR-UFBs remained unchanged. In contrast, CPT induced both type of UFBs, indicating that collapsed forks/DSBs lead to the formation of recombination intermediates that require processing.

To confirm that the UFBs described here are generated by HR, we depleted RAD51 or BRCA2 (Supplementary Fig. 4g). Since inactivation of RAD51 or BRCA2 can also induce replication stress[10, 37], FANCD2-positive and FANCD2-negative UFBs were quantified. Depletion of RAD51 or BRCA2 reduced the number of FANCD2-negative UFBs (i.e. HR-

UFBs), while increasing the FANCD2-positive UFBs (Fig. 3c,d). Expression of RusA[WT]-GEN1, but not RusA[D70N]-GEN1, reduced UFB formation in the resolvase-deficient cells (Fig. 3e,f and Supplementary Fig. 4h,i), further supporting the concept that these UFBs are generated by HR.

HR-UFB breakage promotes DNA damage and chromosome abnormalities

Since UFBs were not observed in resolvase-deficient cells that had completed cytokinesis (Supplementary Fig. 5a), we reasoned that the single-stranded HR-UFBs are likely to be fragile and could be broken by the spindle forces present at mitosis. We therefore determined the levels of DNA damage in the following G1 phase (cyclin A-negative cells) by visualising MDC1 foci (Fig. 4a,b), and found a significant increase in MDC1 foci[38, 39]. DNA damage was dependent on cell division, as treatment with nocodazole and the MPS1 inhibitor reversine, which inhibit spindle assembly and the mitotic checkpoint, rescued the increased number of MDC1 foci (Fig. 4a,b). We also detected elevated levels of cell division-dependent DNA breaks in the resolvase-deficient cells using alkaline comet assays (Supplementary Fig. 5b,c). In contrast, aphidicolin-induced G1 MDC1 foci were not affected by nocodazole and reversine treatment (Supplementary Fig. 5d,e), consistent with previous studies showing that replication stress-induced G1 lesions are transmitted from early mitosis to daughter cells rather than being generated by cell division[38].

To determine whether DNA damage, generated by breakage of the RPA-coated bridges, leads to the cell cycle arrest (Fig. 1b), BrdU-pulse chase experiments were carried out in which cells were briefly exposed to cisplatin for 1 h and, at 12-48h after release, were analysed for their DNA content (Fig. 4c). The resolvase-deficient cells displayed G2 arrest only in the second cell cycle (i.e. 48h after cisplatin release). These results contrast with those obtained after depletion of ERCC1, which is involved in the early stages of ICL unhooking[40, 41], as ERCC1-depleted cells show pronounced G2 arrest 24h after cisplatin release (i.e. in the first cell cycle) (Supplementary Fig. 5f,g). Moreover, resolvase-deficient cells showed high levels of γH2AX, and phosphorylation of the ATM targets CHK2 T68 and KAP-1 S842, 48h after drug release, correlating with the G2/M transition block (Supplementary Fig. 5h). Significant CHK1 pS317 phosphorylation in response to ATR activation was not observed, indicating that cell cycle arrest was induced by DNA breaks rather than by replication checkpoint activation. Furthermore, inhibition of cell division by nocodazole/reversine treatment, which generated tetraploid cells with 8N DNA content, prevented activation of the DNA damage response measured by a reduction in S10 phosphorylation of histone H3 (Supplementary Fig. 6a-c). These results show that HR-UFB breakage is a consequence of cell division, leading to DNA damage in the subsequent cell cycle.

Analysis of metaphase spreads from control and resolvase-deficient cells (24 or 48h after release from cisplatin treatment) revealed that resolvase-deficient cells exhibited an increased frequency of chromosome fusions (end-to-end fusions and radial chromosomes) after approximately two cell cycles (Fig. 4d,e). Inhibition of non-homologous end joining (NHEJ) by the DNA-PKcs inhibitor NU7026 suppressed this fusion phenotype (Fig. 4f). Blocking cell division by nocodazole and reversine also partially rescued the elevated

frequency of chromosome fusions (Fig. 4g). Low levels of fusions also occurred in unchallenged resolvase-deficient cells (Supplementary Fig. 6d).

Resolvase-deficient cells also displayed an increased frequency of mis-segregation events compared with control cells (Supplementary Fig. 6e,f). 24 hours after release from cisplatin, before chromosome fusions were prominent (Fig. 4e), most DAPI-positive anaphase bridges in the resolvase-deficient cells did not contain centromeres, indicating that they were induced by pre-mitotic defects42. After 48 hours the resolvase-deficient cells displayed an elevated frequency of lagging chromosomes with centromeres, which correlates with chromosome fusions (Fig. 4d,e). Inhibition of NHEJ by NU7026 partially rescued the increased frequency of lagging chromosomes with centromeres (Supplementary Fig. 6g). These results show that HR-UFB breakage leads to gross chromosome abnormalities mediated through NHEJ-mediated chromosome fusions.

PICH/BLM promote ssDNA formation at UFBs

To understand how RPA-coated UFBs are generated from unresolved recombination intermediates, the bridges were stained using antibodies against BLM or PICH, a protein required for the recruitment of BLM3, 4, 43, and RPA2 (Fig. 5a-d). In early anaphase, most UFBs were coated with both RPA and PICH/BLM. However, in late anaphase/early telophase some UFBs became only RPA-coated. The UFBs were exclusively RPA2-coated at late telophase, indicating that that duplex DNA bridges are converted to ssDNA, and that PICH/BLM plays a role in their processing.

To determine how single-stranded HR-UFBs arise, we depleted the resolvase-deficient cells for a variety of DNA nucleases (TREX1, MRE11, CTIP, DNA2, EXO1) or helicases (BLM, WRN, RECQ1, RECQ4, RECQ5, RTEL1) and analysed RPA-positive UFB formation. Remarkably, only BLM depletion led to significantly fewer RPA-positive UFBs (Fig. 5e-g, and Supplementary Fig. 7a,b). We therefore generated cell lines expressing either GFP-tagged wild-type or catalytic-dead (BLM^{K695M}) versions of BLM, and treated them with siRNAs against BLM (targeting the 3' UTR of BLM's mRNA), GEN1 and MUS81 (Supplementary Fig. 7c). The GFP-BLM^{K695M}-expressing cells exhibited a significantly reduced frequency of RPA-positive UFBs compared to those expressing GFP-BLM^{WT} (Fig. 6a,b). Moreover, those expressing GFP-BLM^{K695M} showed an increase in the percentage of cells with UFBs that were persistently coated with BLM.

Consistent with a role for BLM in the processing of HR-UFBs, an elevated frequency of PICH-positive UFBs was seen when resolvase-deficient cells were depleted for BLM (Fig. 6c,d). We therefore sought to knock-out PICH to specifically investigate the mitotic functions of BLM, since PICH plays no role in the interphase actions of BLM during DNA replication and repair8, 43. We were, however, unable to make a complete PICH knock-out in the *GEN1*$^{-/-}$ 293 cell line, so instead targeted three out of the four alleles of *PICH* (this cell line is referred to as *GEN1*$^{-/-}$ *PICH*$^{3/4}$), which resulted in reduced PICH expression (Supplementary Fig. 7d,e) and slow growth compared with *GEN1*$^{-/-}$ cells (doubling time of 30h *vs* 22h; Supplementary Fig. 7f). The resolvase-deficient *PICH*$^{3/4}$ cells exhibited a significantly lower frequency of RPA-positive UFBs (Fig. 6e), supporting the hypothesis that

PICH recruits BLM to unwind duplex DNA present in the HR-UFBs to generate the ssDNA bridges.

An inability to convert double stranded bridges to fragile single-stranded UFBs might be expected to lead to cytokinesis failure. We therefore analysed the DNA content of resolvase-deficient $PICH^{3/4}$ cells (Fig. 6f,g), and observed a significant increase in their tetraploid (8N) population compared with PICH-proficient cells. Similarly, it was previously shown that $PICH^{-/-}$ DT40 cells display elevated polyploidy8. These results show that PICH and BLM generate the single-stranded bridges that facilitate cell division.

A general mechanism for UFB processing

Since HR-UFBs and replication stress-induced FS-UFBs both exhibit RPA binding (Fig. 2a and Fig. 3a), we next determined whether ssDNA formation represents a common mechanism of UFB processing. To do this, we induced catenane-dependent centromeric UFBs using the topoisomerase II inhibitor ICRF-193 (Fig. 7a-d) and found that many centromeric UFBs were also converted to ssDNA. There was a clear reduction in the number of RPA-coated centromeric UFBs following depletion of BLM (Fig. 7a,b) or in $PICH^{3/4}$ cells (Fig. 7c,d), as observed previously44. These results indicate that HR-UFBs, FS-UFBs and C-UFBs are processed by a common mechanism involving ssDNA formation and RPA-binding, in order to allow their subsequent breakage and repair.

Discussion

In this work, we described the generation of a resolvase-deficient model that could be used to follow the biological fate of unresolved recombination intermediates at mitosis. We found that HR intermediates fail to elicit a checkpoint response and therefore persist until mitosis where they give rise to a distinct class of UFBs. The interlinked sister chromatids are acted upon by PICH and BLM, and are converted to RPA-coated ssDNA bridges. These HR-UFBs are distinct from replication stress-induced UFBs that are characteristically flanked by FANCD2 foci. However, our data indicate that HR-UFBs, FS-UFBs and C-UFBs all share some common aspects of processing that are necessary for their breakage and results in chromosome segregation and cell division. Disruption of ssDNA formation, by inactivation of the BLM helicase, leads to cytokinesis failure.

Breaking chromosomal DNA requires up to ~100 nN force45 which is ~100 times more than the spindle forces generated by kinetochore fibres (~1 nN)46. However, the force required to break a single covalent bond is 1 - 2 nN47, 48, making it plausible that single-stranded bridges may be sheared by the tensile forces generated by the spindle at mitosis. In contrast to the single-stranded UFBs visualised here at anaphase/telophase, dicentric or lagging chromosomes induce cleavage furrow regression49, 50, or become stabilized as chromatin bridges between daughter cells, and persist for several hours until single-stranded DNA become apparent and breakage occurs15, 50.

Fig. 7e shows a schematic for HR-UFBs processing. PICH recruits BLM helicase to HR-UFBs so it can unwind the duplex DNA into single strands that are broken to allow cell division. Our work shows that HR-UFBs, FS-UFBs and C-UFBs all become decorated with

RPA, dependent upon PICH and BLM, indicating that DNA unwinding by BLM provides a universal mechanism that facilitates bridge resolution/breakage. Whether or not the initial duplex bridge needs to be nicked to allow PICH/BLM access, or whether the tensile force of the spindle generates sufficient force to overstretch and melt the DNA to allow PICH/BLM binding, is presently unknown.

Bridge processing reduces the risk of cytokinesis failure. However, this may occur at the expense of DNA damage and the potential for chromosomal aberrations in the next cell cycle. Indeed, in our resolvase-deficient system we observed high levels of NHEJ-dependent end-to-end chromosome fusions and radial chromosomes, together with an increased frequency of mis-segregation. Since the fusions were not observed when cell division was blocked by nocodazole/reversine treatment, they appear to be products of breakage that occurred in the previous mitosis. The breakage/reunion events observed here are consistent with previous studies showing that NHEJ promotes chromosome abnormalities such as translocations and chromothripsis following a defective mitosis[51, 52].

Chromosomal instability (CIN) is common trait of cancer cells. Cellular defects such as replication stress, merotelic kinetochore attachment and impairment of the cohesion network are known to drive CIN[42, 53, 54]. Our findings reveal that unresolved recombination intermediates may also serve as a potential driver of CIN. Although resolvase-deficiency has not been described in any cancer model, and our model system provides an extreme demonstration of the fate of multiple unresolved recombination intermediates, the work demonstrates the fate of any HR intermediates that escape detection by the dissolution/resolution pathways. This may be particular pertinent to cancer cells where the HR pathway is hyper-activated and the load of recombination intermediates is increased (e.g. when RAD51 activity is elevated)[55–57]. Finally, the synthetic lethal relationship observed between MUS81/SLX4 and GEN1 indicates that resolvases might represent plausible targets for cancer therapies, possibly in combination with DNA damaging agents such as cisplatin. It may therefore be interesting to determine whether tumours that confer resistance to DNA damaging agents due to enhanced HR-mediated repair show a selective sensitivity to resolvase inhibition compared to normal cells.

Methods

Plasmids

GEN1 and GEN1^{EEAA} carrying 3xFLAG tags at their C-termini were cloned into the pcDNA5/FRT/TO vector (Life Technologies) as described[58]. Plasmids encoding RusA^{WT} and RusA^{D70N} (pMW462 and pMW463) were kindly provided by Matthew Whitby (University of Oxford, UK)[59]. RusA^{WT} and RusA^{D70N} sequences were cloned into the N-terminus of GEN1^{EEAA}-3xFLAG using an In-fusion cloning kit (Clontech). To generate the sgRNA vectors for gene targeting, pairs of annealed oligos (see below) were cloned into the pX330 or pX459 plasmids according to published protocols[60,61]. The pEGFP-C2 vector carrying GFP-BLM was a gift from Ian Hickson (University of Copenhagen, Denmark). The catalytic-dead mutant of BLM, BLM^{K695M} was generated by using QuikChange Lightning Multi Site-Directed Mutagenesis kit (Agilent).

The sequences of the sgRNA oligos used for gene targeting were:

GEN1: 5'-CACCGCACATCCCCTTGCGTAATCT-3' and

5'-AAACAGATTACGCAAGGGGATGTGC-3' (ref. 58)

MUS81: 5'-CACCGTCTGAAATACGAAGCGCGTG-3' and

5'-AAACCACGCGCTTCGTATTTCAGAC-3'

SLX1: 5'-CACCGTAGACGCCGAAAAAGCGCCC-3' and

5'-AAACGGGCGCTTTTTCGGCGTCTAC-3'

SLX4: 5'-CACCGCCGGTGCTGAAGAAGGAAC-3' and

5'-AAACGTTCCTTCTTCAGCACCGGC-3'

PICH: 5'-CACCGCCGAAGGTTTCCGGAAGCCG-3' and

5'-AAACCGGCTTCCGGAAACCTTCGGC-3' (ref. 62)

Cell culture and transfection

Flp-In T-REx 293 cells and U2OS cells were cultured in DMEM medium (Life Technologies). eHAP cells (Horizon Discovery)63 were cultured in IMDM medium (Life Technologies). hTERT-RPE1 cells were cultured in DMEM/F-12(1:1) medium (Life Technologies). All of them were grown at 37°C in 5% CO_2. Cultures were supplemented with 10% fetal bovine serum and penicillin/streptomycin. Although initially haploid, the eHAP cell lines have the tendency to stabilize their DNA content at the diploid level, as assayed by FACS, so for consistency diploid clones were selected for all experiments. Geneticin (400 εg/mL), Hygromycin (100 εg/mL), zeocin (50 εg/mL) and blasticidin (4 εg/mL) were obtained from Life Technologies. Nocodazole (100 ng/mL), cisplatin, mitomycin, hydroxyurea (2 mM), reversine (0.5 εM), NU7026 (10 εM), ICRF-193 (0.1 εM) and BrdU (10 or 100 εM) were obtained from Sigma-Aldrich. To generate stable cell lines expressing the RusA/GEN1 proteins, Flp-In T-REx 293 cells were co-transfected with pcDNA5/FRT/TO plasmids encoding the protein of interest, together with the plasmid pOG44 which encodes Flp recombinase (in 1:9 ratio). Hygromycin-resistant colonies were picked and expanded. Protein expression was induced with 10-50 ng/mL of tetracycline (Sigma-Aldrich). To generate stable cell lines expressing BLM, Flp-In T-REx 293 cells were transfected with pEGFP-C2 and geneticin-resistant colonies were picked and expanded.

For gene targeting, cells were transfected with pX330 or PX459 carrying the targeting sequences, together with pSuper.puro (Oligoengine) at a 9:1 ratio. After 24-48 h, cells were selected with 2 εg/mL puromycin, and seeded as single colonies. Clones were picked and first selected on the basis of a negative signal when western blotted. The selected clones were then verified by sequencing. To do this, genomic DNA was extracted from cells with DNeasy Blood & Tissue kit (Qiagen), and PCR was carried out with KOD Hot Start DNA Polymerase (Novagen) to amplify the targeted locus using a forward and a reverse primer

(see below). The PCR product was then purified by QIAquick PCR Purification Kit (Qiagen) and finally sequenced. For genes that have more than two alleles in 293 cells, the PCR products were cloned into pJet vector using CloneJET PCR Cloning Kit (Thermo Fisher). The plasmids were then sequenced to identify mutations in all alleles. To generate endogenous mutations in *SLX4* (E1577A and L1578A), an ssODN template (5'-GTGCTAATCGGAAGAAGAACTTGCCCCCCAAAGTGCCCATAACGCCGATGCCACA GTATTCCATTATGGAGACGCCGGTGCTGAAGAAGGCAGCTGATAGGTTGGCGGTC TTCAAAGCTTGTTGCCCACAGTGGTCTTTTCCCTCCCATAAGTAACTGGGTTTCAC ACACCTGGGGGCGGAAGGGC-3'; Integrated DNA Technologies) was co-transfected (10 ɛL of 10 ɛM for a 60 mm plate) with the sgRNA vector.

The primer sequences used to verify gene targeting were:

GEN1: 5'-GTGGCTTATAATATATTGTTTG-3' and 5'-GCTTTTAGTATCTG AAGCATC-3'; MUS81: 5'-GAATCCCGACTCCAGAACTG-3' and 5'-GCTCGTCCAGCATCCGGCAG-3'; SLX1: 5'-GAGCTTGTTCCGAAGCAAGC-3' and 5'-CGTGCACGACGAGCACCATC-3'; SLX4: 5'-TTACCCAGAAGGTGCTAATCG-3' and 5'-GCCTGGTGTGGTGGCGTGTGC-3'; PICH: 5'-GGAGTGAGCGAAATTCAAGC-3' and 5'-AGACTTAGGGCTTGATAAGC-3'

Cell extracts, immunoprecipitation and Western blotting

Cell lysates were prepared by resuspending cells in Hepes lysis buffer (50 mM Hepes pH 7.4, 150 mM NaCl, 0.1% Triton X-100, 10% glycerol, 1 mM dithiothreitol) supplemented with protease and phosphatase inhibitors. The lysates were incubated on ice for 30 min and then cleared by centrifugation (14,000 rpm, 30 min). For immunoprecipitation, 0.5 µg of antibody was incubated with 0.5 mg of cleared lysate and protein was affinity purified using protein G sepharose (GE Healthcare). The beads were then washed extensively with lysis buffer and analysed by western blotting. For Western blotting of BRCA2 and RAD51, RIPA buffer (50 mM Tris-HCl pH 7.5, 150 mM NaCl, 1% Triton X-100, 0.5% sodium deoxycholate, 0.1% SDS and 5 mM EDTA) was used to lyse the cells.

Proteins were detected by Western blotting using the following primary antibodies: rabbit anti-MRE11 (1:1000, Cell signalling 48955), rabbit anti-DNA2 (1:1000, Abcam ab96488), rabbit anti-EXO1 (1:1000, Abcam ab95068), rabbit anti-CTIP (1:1000, Bethyl A300-488A), rabbit anti-RTEL1 (1:1000, Novus NBP2-22360), rabbit anti-RECQ1 (1:1000, Bethyl A300-447A), rabbit anti-RAD51 (1:200, SantaCruz sc-8349), mouse anti-BRCA2 (1:1000, Calbiochem OP95), mouse anti-α-tubulin (1:5000, sigma T9026), mouse anti-FLAG HRP (1:1000, Sigma-Aldrich A8592), mouse anti-MUS81 (1:1000, Santa Cruz sc-47692), rabbit anti-BLM (1:1000, Abcam ab2179), rabbit anti-KAP-1 pSer842 (1:1000, Abcam ab70369), mouse-anti-CHK1 (1:1000, Sigma-Aldrich C9358), rabbit anti-CHK1 pSer317 (1:1000, Cell signalling 2341), mouse anti-histone H2A.X pSer139 (1:1000, Millipore 05-636-1), mouse anti-CHK2 (1:1000, Millipore 05-649), rabbit anti-CHK2 pThr68 (1:1000, Cell signaling 2661), mouse anti-RPA2 (1:1000, Abcam ab2175), rabbit anti-ERCC1 (1:200, Santa Cruz sc-10785), mouse anti-PICH (1:500, Millipore 04-1540), rabbit anti-GEN1 (1:100, raised against GEN1[890-908])64, sheep anti-SLX1 and sheep anti-SLX4 (1:500, gifts from John Rouse), rabbit anti-WRN, rabbit anti-RECQ4 and rabbit anti-RECQ5 (1:500, gifts from

Pavel Janscak). Primary antibody detection was achieved with IRDye 680RD/800CW-conjugated donkey anti-mouse or anti-rabbit antibodies (LI-COR) and detection by LI-COR Odyssey CLx imaging system (for Supplementary Fig. 3k, 4f,g and 7a), or with HRP-conjugated goat anti-mouse or anti-rabbit antibodies (Dako), or HRP-conjugated rabbit anti-sheep antibody (Abcam) and exposure to Amersham Hyperfilm ECL film (GE Healthcare) (for all the other Western blotting).

Immunofluorescence and EdU labelling

For immunofluorescence analyses, the cells grown on coverslips were fixed with PTEMF buffer (20 mM PIPES pH 6.8, 0.2% Triton X-100, 1 mM $MgCl_2$, 10 mM EGTA and 4% paraformaldehyde) for 10 min. Cells were then permeabilized with 0.2 % Triton X-100 in PBS for 5 min and blocked with 3% BSA/PBS for 30 min. Cells were incubated with primary antibodies diluted in 3% BSA/PBS for 1 h, washed with PBS and incubated with secondary antibodies diluted in 3% BSA/PBS for 1 h. The coverslips were washed twice with PBS and then mounted with Prolong Diamond antifade mountant (Thermo Fisher). The primary antibodies used were: rabbit anti-GFP (1:5000, Abcam ab290), mouse anti-cyclin A (1:200, Santa Cruz sc-56299), rabbit anti-MDC1 (1:1000, Abcam ab11169); mouse anti-RPA2 (1:1000, Abcam ab2175); rabbit anti-RPA2 (1:1000, Abcam ab97594); mouse anti-FLAG (1:1000, Sigma-Aldrich A8592); rabbit anti-BLM (1:1000, Abcam ab 2179), rabbit anti-FANCD2 (1:1000, Novus NB100-182); human anti-centromere CREST (1:1000, Immunovision HCT-0100); rabbit anti-PICH (1:100, Cell Signaling 8886), rabbit anti-TREX1 (1:1000, Abcam ab185288), rabbit anti-MKLP1 (1:1000, Santa Cruz sc-867). Secondary antibodies conjugated to Alexa Fluor 488, Alexa Fluor 555 and Alexa Fluor 647 (1:2000, Thermo Fisher) were used for detection. DNA was stained with DAPI. Images were acquired using Zeiss AXIO Imager M2 microscope with a plan-SPOCHROMAT 63x 1.4 oil objective (Zeiss) and Hamamatsu photonics camera under the control of Volocity software (PerkinElmer). Z stacks were acquired at 0.2 εm intervals and merged images were generated by Volocity software. Deconvulation (Iterative Restoration with 20 iterations) was performed using Volocity software. Images were processed using Adobe Photoshop.

For the detection of UFBs, the cells were treated with siRNA 24 h before a brief cisplatin treatment (1 εM, 1 h), and released into fresh media for 24 h. Cells were then fixed with PTEMF. For the detection of DNA replication in prometaphase, the cells were treated with EdU (10 εM) 30 min before fixation with PTEMF. EdU signals were detected using Click-iT EdU Alexa Fluor 488 Imaging Kit (Life Technologies) according to the manufacturer's protocol.

Flow cytometry

Cells were harvested, washed with PBS and fixed in ice-cold 70% ethanol overnight at 4°C. For DNA content analysis, the cells were washed with PBS and incubated with 50 εL of 100 εg/mL RNase A (Qiagen) and 300 εL of 50 εg/mL propidium iodide (Sigma-Aldrich) prior to FACS analysis. For BrdU staining, cells were treated with 10 εM BrdU for 1 h before being harvested. Fixed cells were washed twice in PBS, treated with 2 N HCl for 20 min, and then washed 2 times in PBS and 1 time in PBS-T (PBS with 0.1% Tween 20 and 0.5 % BSA). Cells were then treated with mouse anti-BrdU antibody (Becton Dickinson) for 30

min at room temperature, washed twice, and stained with anti-mouse Alexa Fluor 488 secondary antibody (Thermo Fisher) for 30 min. For the detection of phosphorylated histone H3 serine 10, ethanol-fixed cells were washed twice in PBS, and once in PBS-T. The cells were then treated with mouse anti-histone H3 pSer10 antibody (Abcam ab14955) for 30 min at room temperature, washed twice, and stained with anti-mouse Alexa Fluor 488 secondary antibody (Thermo Fisher) for 30 min. For the detection of cyclin B1, cells were fixed with 2% paraformaldehyde in PBS for 10 min followed by cold 70% ethanol overnight. Fixed cells were washed twice in PBS, and once in PBS-T. The cells were then treated with mouse anti-cyclin B (Cell signalling 4135) for 30 min at room temperature, washed twice, and stained with anti-mouse Alexa Fluor 488 secondary antibody (Thermo Fisher) for 30 min. Following antibody staining, the cells were then washed with PBS and stained with either propidium iodide (for ethanol-fixed cells) or 0.5 ℮g/mL DAPI (for paraformaldehyde-fixed cells). Samples were run on a FACSCalibur or a LSRFortessa analyzer (BD Biosciences), and at least 10,000 events were acquired per sample. FACS data were analysed using FlowJo software. Cell doublets and debris were excluded form analysis. Cell cycle population analysis was performed using the Watson pragmatic algorithm with FlowJo software.

Comet Assays

Alkaline comet assays were performed using the CometAssay kit from Amsbio (4250-050-K) according to the manufacturer's protocol. Alkaline electrophoresis was performed in a BioRad Mini-Sub Cell GT system (20 volts, 250-300 mA for 30 min), and the comets were stained with SYBR Gold staining solution (Thermo Fisher, 1: 10,000 in TE buffer). The percentage of DNA in the tail was measured using ImageJ software with Comet Assay plugin (https://www.med.unc.edu/microscopy/resources/imagej-plugins-and-macros/comet-assay).

siRNA

The control siRNA (5'-UAAUGUAUUGGAACGCAUA-3'), BLM siRNA (5'-CCGAAUCUCAAUGUACAUAGA-3')[65], RECQ5 siRNA (5'-CAGGAGGCUGAUAAAGGGUUA-3')[65], TREX1 siRNA (5'-CCAAGACCAUCUGCUGUCA-3')[66], CTIP siRNA (5'-GCUAAAACAGGAACGAAUC-3')[67], GEN1 siRNA (5'-GUAAAGACCUGCAAUGUUA-3') were purchased from Eurofins. The MUS81 siRNA (5'-CAGCCCUGGUGGAUCGAUA-3' and 5'-CAUUAAGUGUGGGCGUCUA-3')[68], SLX1 siRNA (5'-UGGACAGACCUGCUGGAGAUU-3')[69], ERCC1 siRNA (SMARTpool ON-TARGET plus L-006311), MRE11 siRNA (SMARTpool ON-TARGET plus L-009271), EXO1 siRNA (SMARTpool ON-TARGET plus L-013120), DNA2 siRNA (SMARTpool ON-TARGET L-026431), RECQ1 siRNA (SMARTpool ON-TARGET plus L-013597), RECQ4 siRNA (SMARTpool ON-TARGET plus L-010559), WRN siRNA (SMARTpool ON-TARGET plus L-010378), BRCA2 siRNA (SMARTpool ON-TARGET plus L-003462) and RAD51 siRNA (SMARTpool ON-TARGET plus L-003530) were purchased from Dharmacon. Cells were seeded one day before siRNA treatment and transfected with 25 nM of siRNA using Lipofectamine RNAiMAX (Life Technologies).

Clonogenic cell survival assay

Cells were first seeded in 6-well plates and transfected with siRNA. One day later, cells were either left untreated or were treated with various concentrations of cisplatin, aphidicolin or camptothecin for 18 h. ~500 cells were seeded in 6-cm plates and maintained in fresh media for ~10 days to allow colony formation. Colonies were stained for ~5 min with 40 mg/mL crystal violet solution (Sigma-Aldrich) containing 20% ethanol. Percent survival was calculated against untreated cells or the control siRNA sample.

Metaphase Spreads

To analyse chromosome aberrations, the cells were treated with siRNA 24 h before a brief cisplatin treatment (1 εg/mL, 1 h), and released into fresh media for 24 or 48 h. Cells were then treated with colcemid (0.2 μg/mL) for 1 h before being harvested, and metaphase chromosomes were prepared as described[68]. Segmented chromosomes were scored as those containing 2 or more indentations per chromosome. For sister chromatid exchange analyses, cells were treated with BrdU (100 εM) for 48 h, and colcemid (0.2 εg/mL) was added 1 h before harvesting. The SCE assay was performed as described[68].

DNA fibre assays

DNA fibre assays were carried out essentially as described[70]. In brief, 293 cells were pulsed with 15 εM CldU (Sigma-Aldrich) for 20 minutes, washed once with media, and labelled with 200 εM IdU (Sigma-Aldrich) for 40 minutes. Cells were trypsinized, resuspended in PBS and placed on ice. Cells were counted, their concentration adjusted to 500,000 cells/mL, and then mixed 1:5 with unlabelled cells. 3 εL of the cell suspension was placed on the top of a glass slide (Superfrost, 90° edges) followed by addition of 9 μL of lysis buffer (0.5% SDS; 200 mM Tris-HCl pH 7.4; 50 mM EDTA) and lysed by moving a pipet in circular motion until the liquid became viscous. The slides were left for 2 minutes before tilting them at a 10-15° angle to allow the viscous cell lysate to run slowly downwards. The slides were fixed in a methanol:acetic acid solution (3:1) for 15 minutes at room temperature and air dried before staining. The DNA fibres were denatured by incubating the slides in 2.5 M HCl solution for 60 minutes. The slides were then washed twice in PBS and blocked in PBS supplemented with 1% BSA for 30 minutes at room temperature. Slides were stained with rat anti-BrdU (Serotec, BU1/75, OBT0030CX; 1:1200 dilution) and mouse anti-BrdU (BD, B44; 1:500 dilution) in PBS/1% BSA for 2 h, and washed twice in PBS before staining with anti-rat Alexa 594 and anti-mouse Alexa 488 (Thermo Fisher, both 1:500 dilutions) in PBS/BSA for 1 h. Slides were washed twice in PBS followed by one wash in H_2O and left to air dry in a dark place. The slides were mounted with Prolong Gold antifade mountant (Thermo Fisher) and images were acquired on a Zeiss AXIO Imager M2 microscope equipped with a plan-SPOCHROMAT 63x 1.4 oil objective (Zeiss) using Volocity software. Images were analysed using ImageJ software.

Statistics and reproducibility

Experiments were not randomized and no blinding was used during analysis of data. No statistical methods were used to predetermine sample size. Sample sizes were determined based on previous experience to obtain statistical significance and reproducibility. All error

bars represent mean ± standard deviation (s.d.) from three independent experiments. Statistical testing was performed using the two-tailed t-test. A P value of 0.05 was considered as a borderline for statistical significance. Each experiment was repeated at least three times with the exception of Supplementary Figs. 2g,h (two experiments were performed), and Fig. 4c, Supplementary Figs 1b, 1d, 2b-d, 3e, 3j, 5a-b, 7b and all western blots (one experiment was performed).

Data availability

Statistics source data for Figs 1–7 and Supplementary Figs 1–7 are provided in Supplementary Table 1. All data supporting the findings of this study are available from the corresponding author on request.

Supplementary Material

Refer to Web version on PubMed Central for supplementary material.

Acknowledgements

References

1. Uhlmann F. SMC complexes: from DNA to chromosomes. Nat Rev Mol Cell Biol. 2016; 17:399–412. [PubMed: 27075410]

2. Chan KL, Hickson ID. New insights into the formation and resolution of ultra-fine anaphase bridges. Sem Cell & Dev Biol. 2011; 22:906–912.

3. Baumann C, Korner R, Hofmann K, Nigg EA. PICH, a centromere-associated SNF2 family ATPase, is regulated by PLK1 and required for the spindle checkpoint. Cell. 2007; 128:101–114. [PubMed: 17218258]

4. Chan KL, North PS, Hickson ID. BLM is required for faithful chromosome segregation and its localization defines a class of ultrafine anaphase bridges. EMBO J. 2007; 26:3397–3409. [PubMed: 17599064]

5. Chan KL, Hickson ID. On the origins of ultra-fine anaphase bridges. Cell Cycle. 2009; 8:3065–3066. [PubMed: 19755843]

6. Germann SM, et al. TopBP1/Dpb11 binds DNA anaphase bridges to prevent genome instability. J Cell Biol. 2014; 204:45–59. [PubMed: 24379413]

7. Liu Y, Nielsen CF, Yao Q, Hickson ID. The origins and processing of ultra fine anaphase DNA bridges. Curr Opin Genet Dev. 2014; 26:1–5. [PubMed: 24795279]

8. Nielsen CF, et al. PICH promotes sister chromatid disjunction and co-operates with topoisomerase II in mitosis. Nat Comms. 2015; 6:8962.

9. Wang LH, Schwarzbam T, Speicher MR, Nigg EA. Persistence of DNA threads in human anaphase cells suggests late completion of sister chromatid decatenation. Chromosoma. 2008; 117:123–135. [PubMed: 17989990]

10. Chan KL, Palmai-Pallag T, Ying SM, Hickson ID. Replication stress induces sister-chromatid bridging at fragile site loci in mitosis. Nat Cell Biol. 2009; 11:753–760. [PubMed: 19465922]

11. Naim V, Rosselli F. The FANC pathway and BLM collaborate during mitosis to prevent micro-nucleation and chromosome abnormalities. Nat Cell Biol. 2009; 11:761–768. [PubMed: 19465921]

12. Naim V, Wilhelm T, Debatisse M, Rosselli F. ERCC1 and MUS81-EME1 promote sister chromatid separation by processing late replication intermediates at common fragile sites during mitosis. Nat Cell Biol. 2013; 15:1008–1015. [PubMed: 23811686]

13. Ying SM, et al. MUS81 promotes common fragile site expression. Nat Cell Biol. 2013; 15:1001–1007. [PubMed: 23811685]

14. Barefield C, Karlseder J. The BLM helicase contributes to telomere maintenance through processing of late-replicating intermediate structures. Nucl Acids Res. 2012; 40:7358–7367. [PubMed: 22576367]

15. Maciejowski J, Li Y, Bosco N, Campbell PJ, de Lange T. Chromothripsis and kataegis induced by telomere crisis. Cell. 2015; 163:1641–1654. [PubMed: 26687355]

16. Nera B, Huang H-S, Lai T, Xu LX. Elevated levels of TRF2 induce telomeric ultrafine anaphase bridges and rapid telomere deletions. Nat Commun. 2015; 6:10132. [PubMed: 26640040]

17. Sarbajna S, Davies D, West SC. Roles of SLX1-SLX4, MUS81-EME1 and GEN1 in avoiding genome instability and mitotic catastrophe. Genes Dev. 2014; 28:1124–1136. [PubMed: 24831703]

18. Wu L, Hickson ID. The Bloom's syndrome helicase suppresses crossing over during homologous recombination. Nature. 2003; 426:870–874. [PubMed: 14685245]

19. Chen XB, et al. Human MUS81-associated endonuclease cleaves Holliday junctions *in vitro*. Mol Cell. 2001; 8:1117–1127. [PubMed: 11741546]

20. Ciccia A, Constantinou A, West SC. Identification and characterization of the human MUS81/EME1 endonuclease. J Biol Chem. 2003; 278:25172–25178. [PubMed: 12721304]

21. Fekairi S, et al. Human SLX4 is a Holliday junction resolvase subunit that binds multiple DNA repair/recombination endonucleases. Cell. 2009; 138:78–89. [PubMed: 19596236]

22. Munoz IM, et al. Coordination of structure-specific nucleases by human SLX4/BTBD12 is required for DNA repair. Mol Cell. 2009; 35:116–127. [PubMed: 19595721]

23. Svendsen JM, et al. Mammalian BTBD12/SLX4 assembles a Holliday junction resolvase and is required for DNA repair. Cell. 2009; 138:63–77. [PubMed: 19596235]

24. Ip SCY, et al. Identification of Holliday junction resolvases from humans and yeast. Nature. 2008; 456:357–361. [PubMed: 19020614]

25. Rass U, et al. Mechanism of Holliday junction resolution by the human GEN1 protein. Genes Dev. 2010; 24:1559–1569. [PubMed: 20634321]

26. Chan YW, West SC. GEN1 promotes Holliday junction resolution by a coordinated nick and counter-nick mechanism. Nucl Acid Res. 2015; 43:10882–10892.

27. Wyatt HDM, Laister RC, Martin SR, Arrowsmith CH, West SC. The SMX DNA repair tri-nuclease. Mol Cell. 2017; 65:848–860. [PubMed: 28257701]

28. Wyatt HDM, Sarbajna S, Matos J, West SC. Coordinated actions of SLX1-SLX4 and MUS81-EME1 for Holliday junction resolution in human cells. Mol Cell source. 2013; 52:234–247.

29. Wechsler T, Newman S, West SC. Aberrant chromosome morphology in human cells defective for Holliday junction resolution. Nature. 2011; 471:642–646. [PubMed: 21399624]

30. Castor D, et al. Cooperative control of Holliday junction resolution and DNA repair by the SLX1 and MUS81-EME1 nucleases. Mol Cell. 2013; 52:221–233. [PubMed: 24076219]

31. Garner E, Kim Y, Lach FP, Kottemann MC, Smogorzewska A. Human GEN1 and the SLX4-associated nucleases MUS81 and SLX1 are essential for the resolution of replication-induced Holliday junctions. Cell Rep. 2013; 5:207–215. [PubMed: 24080495]

32. Duda H, et al. A mechanism for controlled breakage of under-replicated chromosomes during mitosis. Dev Cell. 2016; 39:740–755. [PubMed: 27997828]

33. Matos J, Blanco MG, Maslen SL, Skehel JM, West SC. Regulatory control of the resolution of DNA recombination intermediates during meiosis and mitosis. Cell. 2011; 147:158–172. [PubMed: 21962513]

34. Chan YW, West SC. Spatial control of the GEN1 Holliday junction resolvase ensures genome stability. Nat Comms. 2014; 5:5844.

35. Nair N, Castor D, Macartney T, Rouse J. Identification and characterization of MUS81 point mutations that abolish interaction with the SLX4 scaffold protein. DNA Rep. 2014; 24:131–137.

36. Minocherhomji S, et al. Replication stress activates DNA repair synthesis in mitosis. Nature. 2015; 528:286–290. [PubMed: 26633632]

37. Schlacher K, et al. Double-strand break repair-independent role for BRCA2 in blocking stalled replication fork degradation by MRE11. Cell. 2011; 145:529–542. [PubMed: 21565612]

38. Lukas C, et al. 53BP1 nuclear bodies form around DNA lesions generated by mitotic transmission of chromosomes under replication stress. Nat Cell Biol. 2011; 13:243–253. [PubMed: 21317883]

39. Harrigan JA, et al. Replication stress induces 53BP1-containing OPT domains in G1 cells. J Cell Biol. 2011; 193:97–108. [PubMed: 21444690]

40. Klein Douwel D, et al. XPF-ERCC1 acts in unhooking DNA interstrand crosslinks in cooperation with FANCD2 and FANCP/SLX4. Mol Cell. 2014; 54:460–471. [PubMed: 24726325]

41. Hodskinson MRG, et al. Mouse SLX4 is a tumour suppressor that stimulates the activity of the nuclease XPF-ERCC1 in DNA crosslink repair. Mol Cell. 2014; 54:472–484. [PubMed: 24726326]

42. Burrell RA, et al. Replication stress links structural and numerical cancer chromosomal instability. Nature. 2013; 494:492–496. [PubMed: 23446422]

43. Ke Y, et al. PICH and BLM limit histone association with anaphase centromeric threads and promote their resolution. EMBO J. 2011; 30:3309–3321. [PubMed: 21743438]

44. Hengeveld RC, et al. Rif1 Is required for resolution of ultrafine DNA bridges in anaphase to ensure genomic stability. Dev Cell. 2015; 34:466–474. [PubMed: 26256213]

45. Houchmandzadeh B, Marko JF, Chatenay D, Libchaber A. Elasticity and structure of eukaryote chromosomes studied by micromanipulation and micropipette aspiration. J Cell Biol. 1997; 139:1–12. [PubMed: 9314524]

46. Alexander SP, Rieder CL. Chromosome motion during attachment to the vertebrate spindle: initial saltatory-like behavior of chromosomes and quantitative analysis of force production by nascent kinetochore fibers. J Cell Biol. 1991; 113:805–815. [PubMed: 2026651]

47. Grandbois M, Beyer M, Rief M, Clausen-Schaumann H, Gaub HE. How strong is a covalent bond? Science. 1999; 283:1727–1730. [PubMed: 10073936]

48. Bustamante C, Smith SB, Liphardt J, Smith DR. Single-molecule studies of DNA molecules. Curr Opin Struct Biol. 2000; 10:279–285. [PubMed: 10851197]

49. Mullins JM, Biesele JJ. Terminal phase of cytokinesis in D-98s cells. J Cell Biol. 1977; 73:672–684. [PubMed: 873994]

50. Steigemann P, et al. Aurora B-mediated abscission checkpoint protects against tetraploidization. Cell. 2009; 136:473–484. [PubMed: 19203582]

51. Janssen A, van der Burg M, Szuhai K, Kops GJ, Medema RH. Chromosome segregation errors as a cause of DNA damage and structural chromosome aberrations. Science. 2011; 333:1895–1898. [PubMed: 21960636]

52. Ly P, et al. Selective Y centromere inactivation triggers chromosome shattering in micronuclei and repair by non-homologous end joining. Nat Cell Biol. 2017; 19:68–75. [PubMed: 27918550]

53. Thompson SL, Compton DA. Examining the link between chromosomal instability and aneuploidy in human cells. J Cell Biol. 2008; 180:665–672. [PubMed: 18283116]

54. Tanno Y, et al. The inner centromere-shugoshin network prevents chromosomal instability. Science. 2015; 349:1237–1240. [PubMed: 26359403]

55. Raderschall E, et al. Formation of higher-order nuclear RAD51 structures is functionally linked to p21 expression and protection from DNA damage-induced apoptosis. J Cell Sci. 2002; 115:153–164. [PubMed: 11801733]

56. Klein HL. The consequences of RAD51 overexpression for normal and tumor cells. DNA Repair. 2008; 7:686–693. [PubMed: 18243065]

57. Marsden CG, et al. The tumor-associated variant RAD51 G151D induces a hyper-recombination phenotype. PLoS Genet. 2016; 12:e1006208. [PubMed: 27513445]

58. Chan YW, West SC. Spatial control of the GEN1 Holliday junction resolvase ensures genome stability. Nat Comms. 2014; 5:5844.

59. Rodriguez-Lopez AM, Whitby MC, Borer CM, Bachler MA, Cox LS. Correction of proliferation and drug sensitivity defects in the progeriod Werner's Syndrome by Holliday junction resolution. Rejuvenation Res. 2007; 10:27–40. [PubMed: 17378750]

60. Cong L, et al. Multiplex genome engineering using CRISPR/Cas systems. Science. 2013; 339:819–823. [PubMed: 23287718]

61. Ran FA, et al. Genome engineering using the CRISPR-Cas9 system. Nat Protoc. 2013; 8:2281–2308. [PubMed: 24157548]

62. Nielsen CF, et al. PICH promotes sister chromatid disjunction and co-operates with topoisomerase II in mitosis. Nat Comms. 2015; 6:8962.

63. Essletzbichler P, et al. Megabase-scale deletion using CRISPR/Cas9 to generate a fully haploid human cell line. Genome Res. 2014; 24:2059–2065. [PubMed: 25373145]

64. Rass U, et al. Mechanism of Holliday junction resolution by the human GEN1 protein. Genes Dev. 2010; 24:1559–1569. [PubMed: 20634321]

65. Paliwal S, Kanagaraj R, Sturzenegger A, Burdova K, Janscak P. Human RECQ5 helicase promotes repair of DNA double-strand breaks by synthesis-dependent strand annealing. Nucl Acids Res. 2013; 42:2380–2390. [PubMed: 24319145]

66. Chowdhury D, et al. The exonuclease TREX1 is in the SET complex and acts in concert with NM23-H1 to degrade DNA during granzyme A-mediated cell death. Mol Cell. 2006; 23:133–142. [PubMed: 16818237]

67. Fugger K, et al. Human FBH1 helicase contributes to genome maintenance via pro- and anti-recombinase activities. J Cell Biol. 2009; 186:655–663. [PubMed: 19736316]

68. Wechsler T, Newman S, West SC. Aberrant chromosome morphology in human cells defective for Holliday junction resolution. Nature. 2011; 471:642–646. [PubMed: 21399624]

69. Munoz IM, et al. Coordination of structure-specific nucleases by human SLX4/BTBD12 is required for DNA repair. Mol Cell. 2009; 35:116–127. [PubMed: 19595721]

70. Petermann E, Orta ML, Issaeva N, Schultz N, Helleday T. Hydroxyurea-stalled replication forks become progressively inactivated and require two different RAD51-mediated pathways for restart and repair. Mol Cell. 2010; 37:492–502. [PubMed: 20188668]
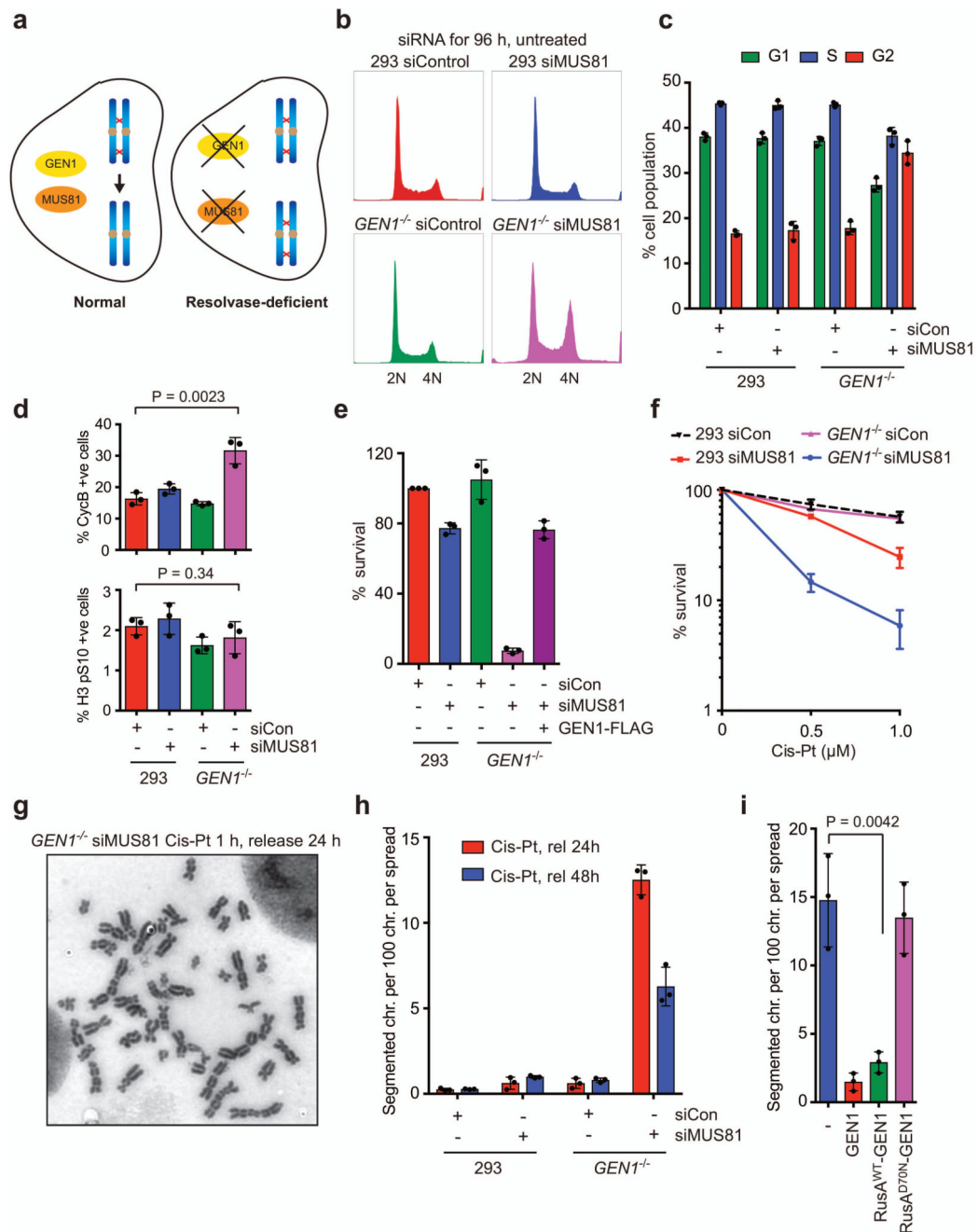
Figure 1. Phenotypic analysis of resolvase-deficient cells.

(a) Schematic diagram depicting the experimental system.

(b) 293 cells and *GEN1*^{-/-} cells were treated with control siRNA or siRNA against MUS81 for 96 h. FACS analyses show their DNA content distributions.

(c) Quantification of G1, S and G2 populations of cells treated as in (b).

(d) Cells were treated as in (b) and stained with cyclin B antibody (upper panel) or histone H3 pSer10 antibody (lower panel). Percentages of cyclin B-positive and histone H3 pSer-positive cells were quantified.

(e) Clonogenic cell survival assays were carried out on 293 cells and *GEN1*$^{-/-}$ cells treated with control siRNA or siRNA against MUS81. Complementation by stable expression of GEN1-3xFLAG is indicated. The survival of control siRNA-treated 293 cells is defined as 100%.

(f) Clonogenic cell survival assays were carried out on 293 and *GEN1*$^{-/-}$ cells treated with control siRNA or siRNA against MUS81, and the indicated concentrations of cisplatin (Cis-Pt).

(g) Chromosome segmentation in a metaphase spread from *GEN1*$^{-/-}$ cells treated with siRNA against MUS81 and a brief cisplatin treatment, and released into fresh media for 24 h.

(h) 293 cells and *GEN1*$^{-/-}$ cells were treated as in (g). 75 metaphase spreads per condition were analysed for chromosome segmentation.

(i) *GEN1*$^{-/-}$ and *GEN1*$^{-/-}$ cells expressing GEN1, RusA^{WT}-GEN1 or RusA^{D70N}-GEN1 were treated as in (g). 60 metaphase spreads per condition were analysed for chromosome segmentation.

In **b** and **g**, representative data from three independent experiments are shown. Quantified data in **c-f**, **h** and **i** represent the mean ± s.d. of n = 3 independent experiments. Source data are available in Supplementary Table 1. P values were determined using a two-tailed t-test.
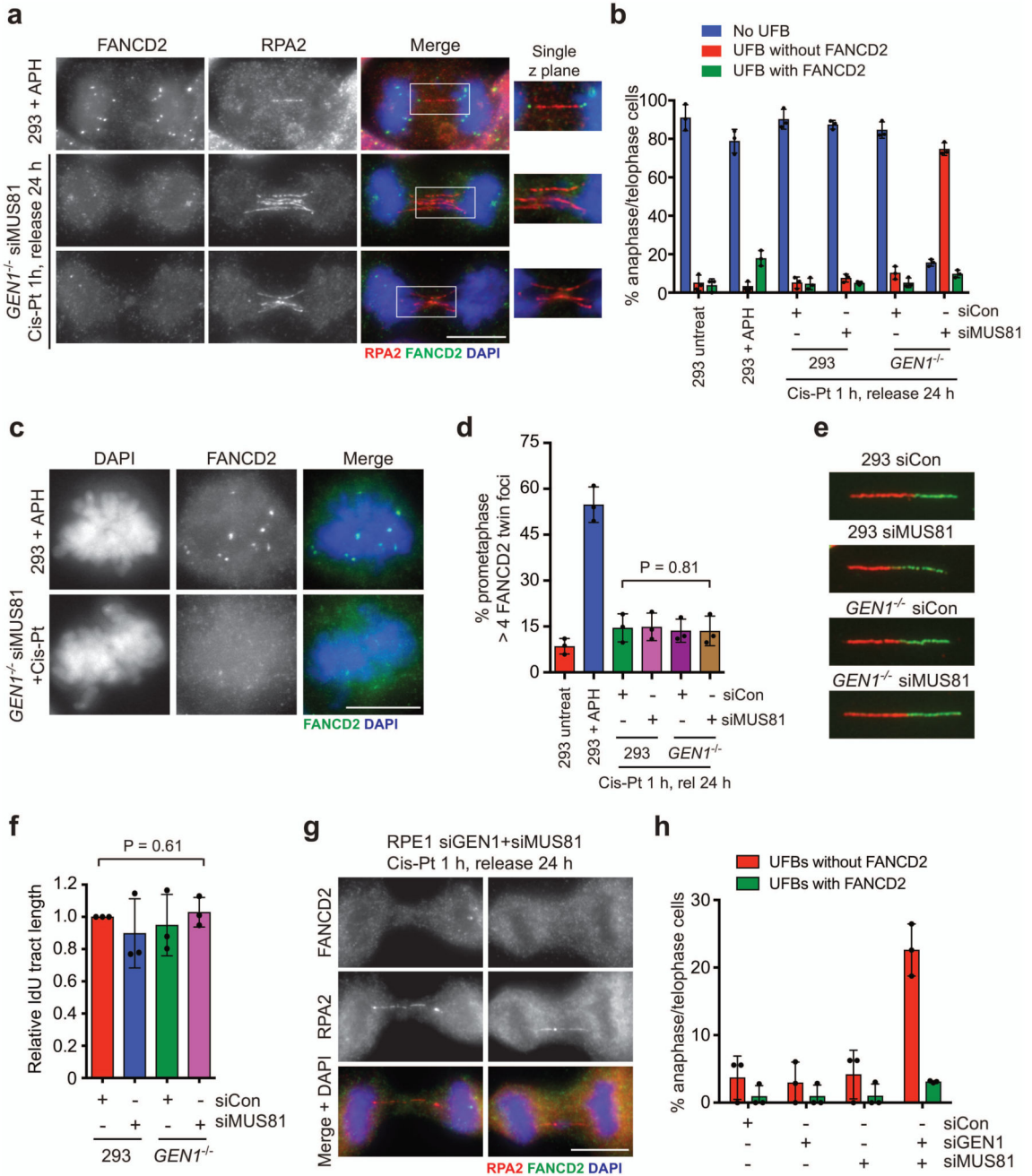
Figure 2. Persistent recombination intermediates lead to the formation of HR-UFBs.
(a) 293 and *GEN1*^{−/−} cells were treated with control siRNA or siRNA against MUS81 and Cis-Pt. 293 cells treated with aphidicolin (APH, 0.2 εM for 16 h) were used as controls. RPA2, FANCD2 and DNA were visualized using anti-RPA2 antibody (red), anti-FANCD2 antibody (green) and DAPI (blue), respectively. Deconvoluted images are shown. Boxed regions are enlarged and single Z planes are shown in the right.
(b) Quantification of anaphase/telophase cells with RPA2-positive UFBs (150 cells per condition), with or without FANCD2 foci, as visualized in (a).

(c) Cells were treated as in (a), and FANCD2 and DNA were visualized using anti-FANCD2 antibody (green) and DAPI (blue), respectively. Deconvoluted images are shown.

(d) Quantification of prometaphase cells with >4 FANCD2 twin foci (150 cells per condition), as visualized in (c).

(e) 293 cells and *GEN1*$^{-/-}$ cells were treated with control siRNA or siRNA against MUS81 for 48 h, and then labelled with CldU and IdU for DNA fibre analysis. Representative fibres are shown.

(f) Quantification of IdU track length relative to 293 control cells (>200 fibres per condition), as in (e).

(g) Representative images of hTERT-RPE1 cells treated with siRNAs against GEN1 and MUS81, and Cis-Pt. RPA2, FANCD2 and DNA were visualized using anti-RPA2 antibody (red), anti-FANCD2 antibody (green) and DAPI (blue), respectively.

(h) Quantification of anaphase/telophase hTERT-RPE1 cells treated with control siRNA, siRNA against GEN1 and/or MUS81, and Cis-Pt. Cells with RPA2-UFBs were classified as with or without FANCD2 foci (>100 cells per condition).

In **a**, **c**, **e** and **g**, representative images of three independent experiments are shown. Quantified data in **b**, **d**, **f** and **h** represent the mean ± s.d. of n = 3 independent experiments. Source data are available in Supplementary Table 1. P values were determined using a two-tailed t-test. Scale bars, 10 μm.
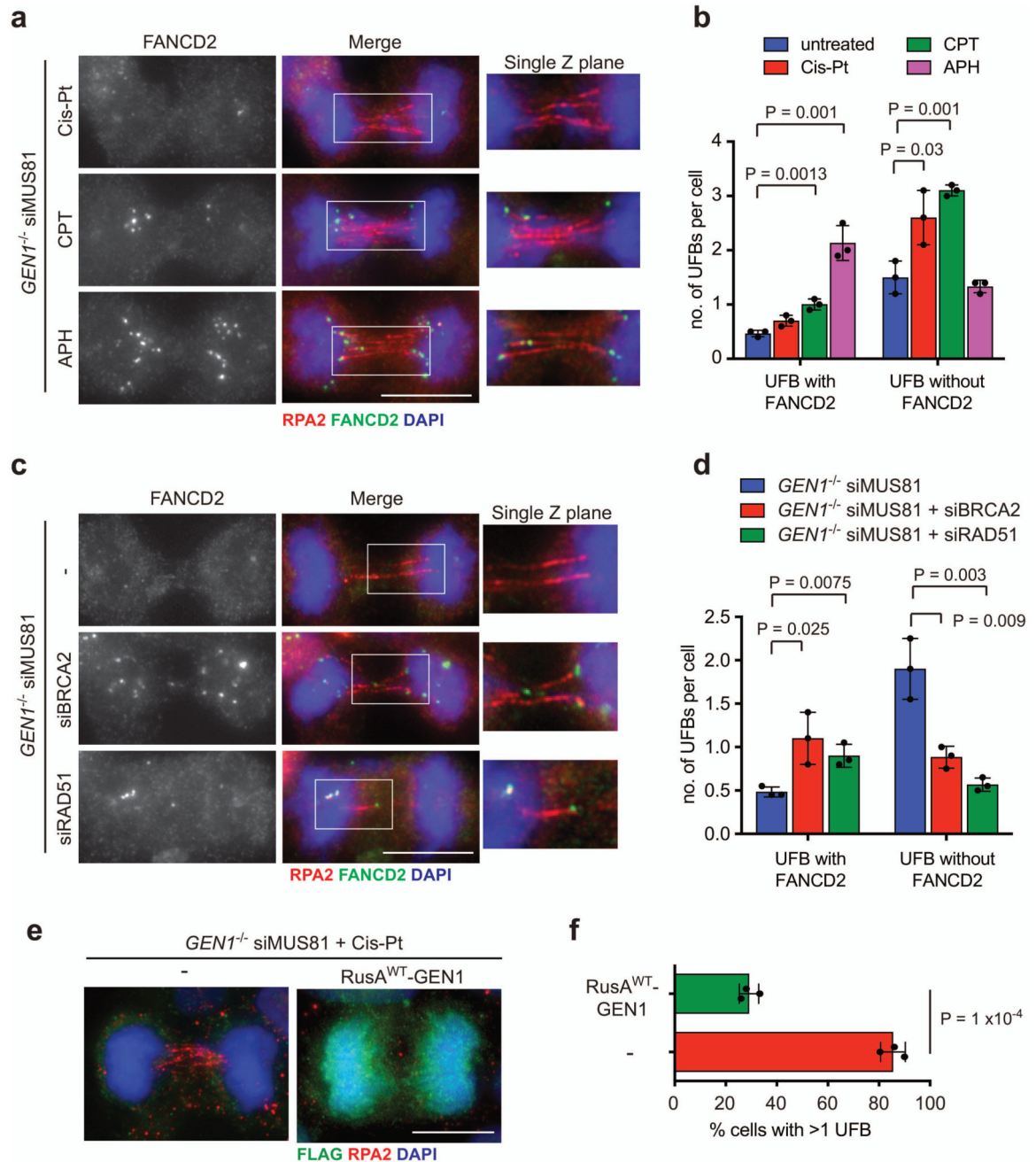
Figure 3. Generation of UFBs by HR in resolvase-deficient cells.
(a) *GEN1*⁻/⁻ cells were treated with siRNA against MUS81. They were then either untreated, or treated with Cis-Pt (1 εM for 1 h and release for 24 h), camptothecin (CPT, 1 εM for 1 h and release for 24 h) or APH (0.2 εM for 16 h). RPA2, FANCD2 and DNA were visualized as indicated. Deconvoluted images are shown. Boxed regions are enlarged and single Z planes are shown in the right.

(b) Quantification of anaphase/telophase cells (30 cells per condition) with RPA2-positive UFBs, classified as with or without FANCD2 foci, as visualized in (a).

(c) *GEN1$^{-/-}$* cells were treated with siRNA against MUS81 alone or together with siRNA against BRCA2 or RAD51 for 72 h. RPA2, FANCD2 and DNA were visualized as indicated. Deconvoluted images are shown. Boxed regions are enlarged and single Z planes are shown in the right.

(d) Quantification of anaphase/telophase cells (60 cells per condition) with RPA2-positive UFBs, classified as with or without FANCD2 foci, as visualized in (c).

(e) *GEN1$^{-/-}$* cells, and *GEN1$^{-/-}$* cells stably expressing RusA^{WT}-GEN1, were treated with siRNA against MUS81 and Cis-Pt. RPA2, RusA^{WT}-GEN1 and DNA were visualized using anti-RPA2 antibody (red), anti-FLAG antibody (green) and DAPI (blue), respectively. Deconvoluted images are shown.

(f) Quantification of cells (> 150 cells per condition) with RPA2-positive UFBs, as visualized in (e).

In **a**, **c** and **e**, representative images of three independent experiments are shown. Quantified data in **b**, **d** and **f** represent the mean ± s.d. of n = 3 independent experiments. Source data are available in Supplementary Table 1. P values were determined using a two-tailed t-test. Scale bars, 10 μm.

Figure 4. HR-UFB breakage leads to DNA damage and gross chromosome abnormalities.
(**a**) 293 cells, and *GEN1⁻/⁻* cells, were treated with control siRNA or siRNA against MUS81 and Cis-Pt, and released into fresh media with or without nocodazole (Noc, 100 ng/mL) and reversine (Rev, 0.5 εM) for 24 h. MDC1, Cyclin A, and DNA were visualized using anti-MDC1 antibody (green), anti-cyclin A antibody (red), and DAPI (blue), respectively. Scale bar, 10 μm.

(**b**) Quantification of G1 cells (>400 cells per condition) with >4 MDC1 foci, as in (a).

(c) 293 cells and *GEN1*$^{-/-}$ cells were treated with control siRNA or siRNA against MUS81, followed by Cis-Pt (1 εg/mL) and BrdU (10 εM) treatment for 1 h. Cells were released into fresh media, collected at the indicated time points and analysed by FACS. The DNA content histograms of BrdU-negative mock-depleted 293 cells, MUS81-depleted 293 cells, mock-depleted *GEN1*$^{-/-}$ cells and MUS81-depleted *GEN1*$^{-/-}$ cells, at the indicated time points are shown.

(d) Representative images of metaphase spreads from *GEN1*$^{-/-}$ cells treated with siRNA against MUS81 and Cis-Pt, and released into fresh media for 48 h. Representative end-to-end fusions and radials are shown.

(e) 293 and *GEN1*$^{-/-}$ cells were treated as in (d), and 75 metaphase spreads per condition were analysed for chromosome fusions in three independent experiments.

(f) *GEN1*$^{-/-}$ cells were treated as in (d), except that DMSO or the DNA-PK inhibitor NU7026 (10 εM) were added 24 h before harvest. Control siRNA-treated 293 cells were used as control. 60 metaphase spreads per condition were analysed for chromosome fusions.

(g) Cells were treated as in (f) except Noc and Rev were added to the cells instead of NU7026. 45 metaphase spreads per condition were analysed in three independent experiments.

In **a** and **d**, representative images of three independent experiments are shown. Quantified data in **b** and **e-g** represent the mean ± s.d. of n = 3 independent experiments. Source data are available in Supplementary Table 1. P values were determined using a two-tailed t-test.
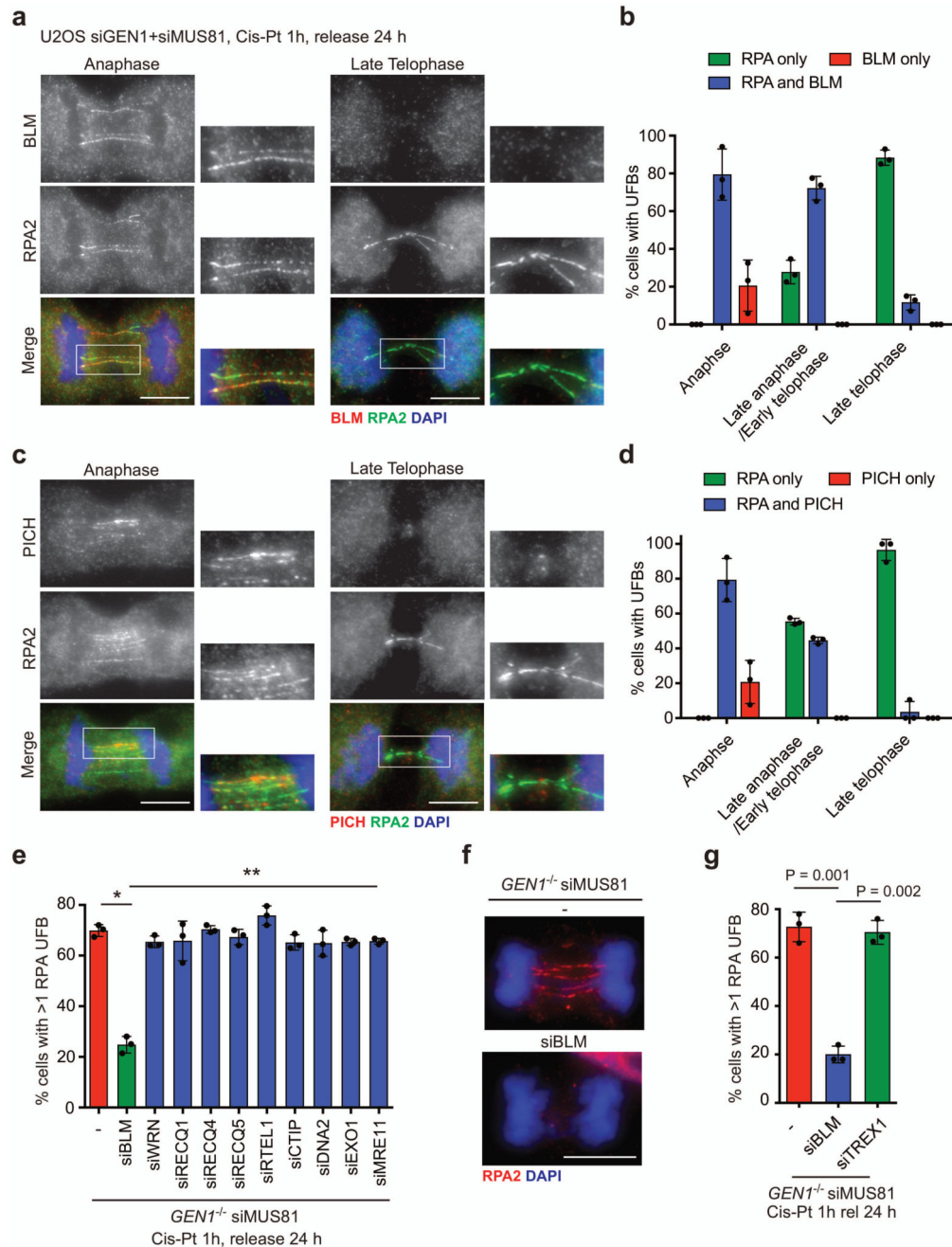
Figure 5. BLM is required for the formation of RPA-coated UFBs.

(a) U2OS cells were treated with siRNA against GEN1 and MUS81, and Cis-Pt. Cells with UFBs in different stages of mitosis were counted. BLM, RPA2 and DNA were visualized as indicated. Deconvoluted images are shown. Boxed regions are enlarged.

(b) Quantification of cells with UFBs (>250 cells counted) as in (a).

(c) U2OS cells were treated as in (a). PICH, RPA2 and DNA were visualized as indicated and deconvoluted images are shown. Boxed regions are enlarged.

(d) Quantification of cells with UFBs (>250 cells counted) as in (c).

(e) *GEN1$^{-/-}$* cells were (>150 cells per condition) treated with siRNA against MUS81 alone, or together with the indicated siRNAs in which various nucleases/helicases were targeted, and Cis-Pt. The percentages of resolvase-deficient cells at anaphase/telophase with RPA2-positive UFBs were determined.

(f) *GEN1$^{-/-}$* cells were treated with siRNA against MUS81 alone, or together with siRNA against BLM, and Cis-Pt. RPA2 and DNA were visualized as indicated.

(g) Quantification of anaphase/telophase cells (>150 cells per condition) with RPA2-positive UFBs. *GEN1$^{-/-}$* cells were treated with siRNA against MUS81 alone, or together with siRNA against BLM or TREX1, and Cis-Pt.

In **a**, **c** and **f**, representative images of three independent experiments are shown. Quantified data in **b**, **d**, **e** and **g** represent the mean ± s.d. of n = 3 independent experiments. Source data are available in Supplementary Table 1. P values were determined using a two-tailed t-test, *P = 4 × 10^{-5}, **P < 0.002. Scale bars, 10 em.
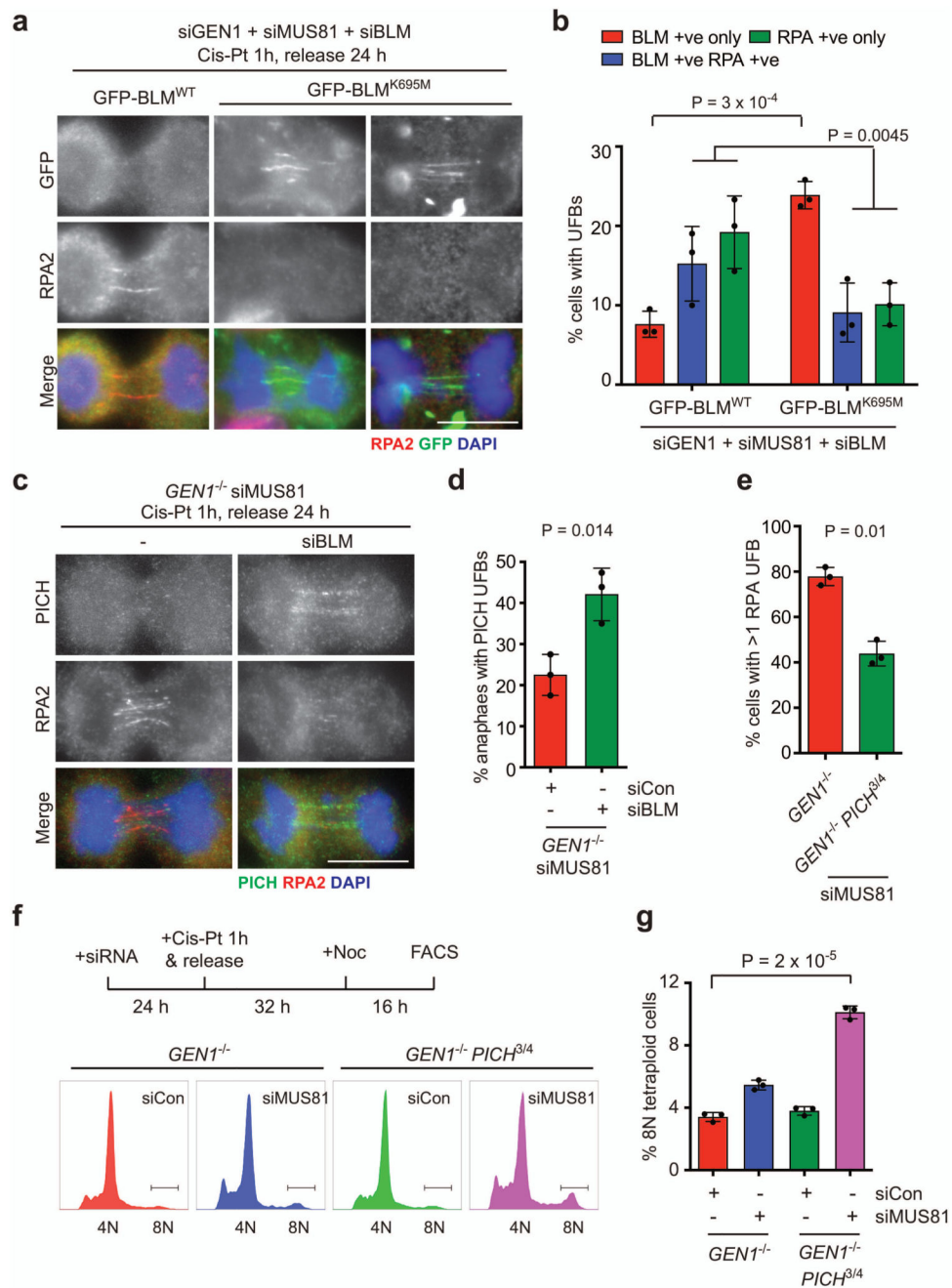
Figure 6. Unwinding of UFBs by PICH/BLM facilitates cell division.
(a) 293 cells stably expressing GFP-BLM^{WT} and GFP-BLM^{K695M} were treated with siRNAs against GEN1, MUS81 and BLM, and Cis-Pt. RPA2, BLM and DNA were visualized using anti-RPA2 antibody (red), anti-GFP antibody (green) and DAPI (blue), respectively.

(b) Quantification of cells (>100 cells per condition) with UFBs shown in (a).

(c) *GEN1*$^{-/-}$ cells were treated with siRNA against MUS81 alone or together with siRNA against BLM, and Cis-Pt. RPA2, PICH and DNA were visualized using anti-RPA2 antibody

(red), anti-PICH antibody (green) and DAPI (blue), respectively. Deconvulated images are shown.

(d) Quantification of anaphase cells with PICH-positive UFBs (>120 cells per condition), as visualized in (c).

(e) *GEN1*$^{-/-}$ cells and *GEN1*$^{-/-}$ *PICH*$^{3/4}$ cells were treated with siRNA against MUS81 and Cis-Pt. The number of cells with RPA2-positive UFBs was quantified (>150 cells per condition).

(f) *GEN1*$^{-/-}$ and *GEN1*$^{-/-}$ *PICH*$^{3/4}$ cells were treated as shown in the scheme (upper panel) and their DNA content distributions were determined by FACS analysis (lower panel).

(g) The percentage of cells with 8N DNA content, as determined in (d), was quantified.

In **a**, **c** and **f**, representative data of three independent experiments are shown. Quantified data in **b**, **d**, **e** and **g** represent the mean ± s.d. of n = 3 independent experiments. Source data are available in Supplementary Table 1. P values were determined using a two-tailed t-test. Scale bars, 10 ɛm.
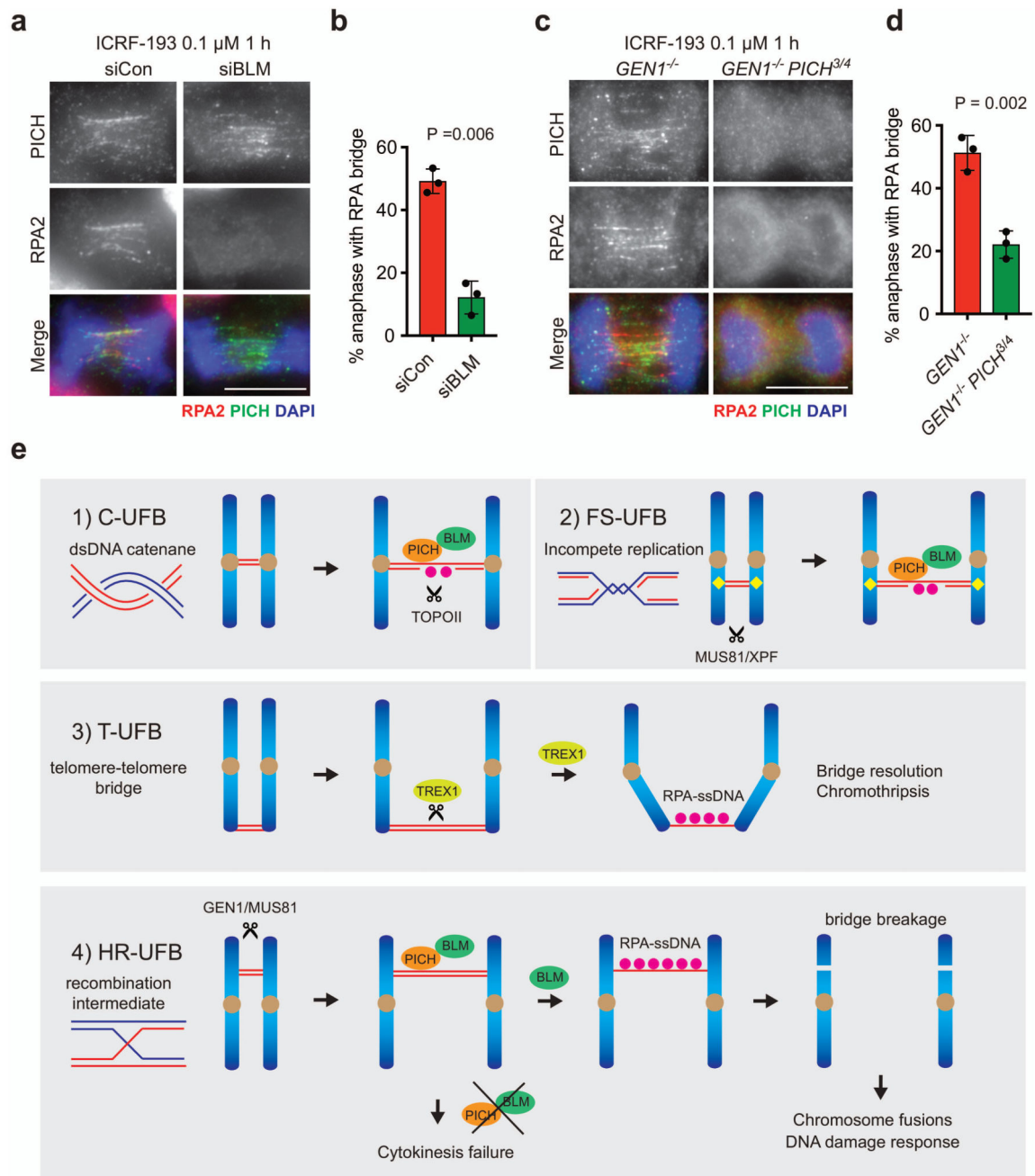
Figure 7. General mechanism for the formation of single-stranded UFBs.

(a) 293 cells were treated control siRNA or siRNA against BLM, and ICRF-193 (0.1 εM, 1 h). PICH, RPA2 and DNA were visualized as indicated.

(b) Quantification of cells (>100 cells per condition) with RPA2-coated UFBs in (a).

(c) $GEN1^{-/-}$ cells and $GEN1^{-/-}$ $PICH^{3/4}$ cells were treated with ICRF-193 (0.1 εM, 1 h). PICH, RPA2 and DNA were visualized.

(d) Quantification of cells (>120 cells per condition) with RPA2-coated UFBs in (c).

(e) Schematic diagram of the four types of anaphase UFB: 1) Centromere-UFBs (C-UFBs) emerge from centromeric regions, possess double-stranded catenanes and are resolved by PICH/BLM and topoisomerase II. Recruitment of BLM is required for RPA formation; 2) Fragile Site UFBs (FS-UFBs) emerge from incompletely replicated DNA at CFSs (yellow rhombus) and are flanked by FANCD2 twin foci. The bridges frequently possess regions that are bound by RPA; 3) Telomere-UFBs (T-UFBs) originate from telomere fusions, persist and develop into chromatin bridges that are processed by TREX1 to ultimately generate ssDNA; 4) Homologous recombination-UFBs (HR-UFBs) originate from unresolved recombination intermediates. In the absence of GEN1/MUS81, HR-UFBs accumulate at anaphase and PICH/BLM are recruited for DNA unwinding, ssDNA formation and breakage at mitosis. See text for further details.

In **a** and **c**, representative images of three independent experiments are shown. Quantified data in **b** and **d** represent the mean ± s.d. of n = 3 independent experiments. Source data are available in Supplementary Table 1. P values were determined using a two-tailed t-test. Scale bars, 10 ɛm.